

# VISIBILITY PARAMETERIZATIONS FOR FORECASTING APPLICATIONS

*I. Gultepe<sup>1</sup>, J. Milbrandt<sup>2</sup>, S. Benjamin<sup>3</sup>, G. A. Isaac<sup>1</sup>, S. G. Cober<sup>1</sup>, and B. Hansen<sup>1</sup>*

<sup>1</sup> *Cloud Physics and Severe Weather Research Section, Science and Technology Branch, Environment Canada, 4905 Dufferin Street, Downsview, Ontario, Canada, M3H 5T4, Canada.*

<sup>2</sup> *Numerical Weather Prediction Research Section, Science and Technology Branch, Environment Canada, Dorval, Quebec, Canada*

<sup>3</sup> *NOAA Earth System Research Laboratory, R/E/GSD, 325 Broadway, Boulder, CO 80305, USA*

## 1. INTRODUCTION

Fog and its effect on visibility (*Vis*) play an important role in our daily life. The total economic loss associated with the impact of fog on aviation, marine and land transportation can be comparable to those of winter storms. For example, in the pre-Christmas period of December 20-23, 2006, the British Airport Authority (BAA) reported that a blanket of fog and freezing fog over the UK forced 175,000 passengers to miss flights from its seven British airports, with Heathrow the worst affected. Early estimates suggested this disruption to air travel cost British Airways at least £25 million (Gadher and Baird, 2007). The costs to stranded passengers in terms of money and inconvenience may be impossible to calculate but it is certainly significant.

In Canada, approximately 50 people per year die due to fog-related motor vehicle accidents (Gultepe et al., 2007). Westcott (2007) stated that approximately 30 deaths occur annually under foggy conditions in Illinois, excluding the city of Chicago. In Europe, a major fog research project called COST-722 (COoperation in Field of Scientific and Technical Research), with objectives of reducing economic and human life losses, was undertaken to develop advanced methods for very short-range forecasts of fog and low clouds (Jacobs et al., 2007). In collaboration with COST-722, Gultepe et al (2008) performed three field projects to study warm fog conditions and developed microphysical parameterization suitable for application to fog and precipitation measurements.

Fog can form over various time and space scales but not all models can resolve small time and space scales e.g. minutes and meters, respectively. Therefore, high-resolution models have been developed to better nowcast fog (Bott et al., 1990). Unfortunately, high-resolution models are not always available; therefore visibility parameterizations have been used in forecasting models.

<sup>1</sup> *Corresponding author email: [ismail.gultepe@ec.gc.ca](mailto:ismail.gultepe@ec.gc.ca)*

There are several *Vis* parameterizations for hydrometeor types e.g. rain and snow (Rasmussen et al., 1999). Fog does not always occur alone but it is associated with other meteorological hydrometers such as rain or snow. Therefore, *Vis* parameterizations should include the visibility from relative humidity with respect to water ( $RH_w$ ), fog (water or ice), and precipitation-related hydrometeors.

In this work, observations collected during the Fog Remote sensing And Modeling (FRAM) field projects (Gultepe et al., 2008) were analyzed to develop *Vis* parameterizations. A model simulation was performed using the GEM-REG (Côté et al., 1998) for an “only fog” case (Fig. 1), without rain, which occurred in eastern Canada near Lunenburg Nova Scotia. In this case, the fog occurrence was mainly related to warm air advection from the Atlantic Ocean over the project area. In addition, several parameterizations are suggested for liquid fog, ice fog, *RH*, rain, and snow. Finally their integration together is discussed along with the associated uncertainty.



Fig. 1: Marine fog as occurred over Lunenburg port on April 18 2006 during the FRAM field project.

## 2. VIS DEFINITIONS

### *a) Daytime definition of Vis*

Meteorological Observation Range (MOR) definition by the World Meteorological Organization (WMO) is based on Koschmieder law. Assuming a brightness contrast threshold ( $\epsilon$ ) as 0.05, daytime visibility ( $Vis_d$ ) is given as

$$Vis_{d5} = 2.996\beta_{ext}^{-1}, \quad (1)$$

where  $\ln(1/\varepsilon)=2.996$ .  $\beta_{ext}$  is the extinction coefficient given as

$$\beta_{ext} = \sum_{i=1}^m \pi Q_{ext}(r)n(r)r^2 dr, \quad (2)$$

where  $Q_{ext}$  is the extinction efficiency and equals  $\sim 2$  for large particles. For ice crystals, it depends on particle shape, particle spectra, and visible light wavelength.

Using  $\varepsilon=0.02$  (threshold of luminance contrast or brightness contrast), Eq. 1 is also given as

$$Vis_{d2} = 3.912\beta_{ext}^{-1}. \quad (3)$$

where  $\varepsilon$  is defined as  $(B_r - B_b)/B_b$ ,  $B_r$  is the apparent luminance of the object at range  $R$  (known) and  $B_b$  is the apparent luminance of the background of the object at range  $R$  (known). In the Rapid Update Cycle (RUC) model (Benjamin et al., 2004)  $Vis$  is obtained by setting  $\varepsilon=0.02$  so that  $Vis_{d5}$  is based on the WMO MOR definition as

$$Vis_{d2} = 1.3Vis_{d5}. \quad (4)$$

In general, measurements from  $Vis$  sensors (e.g. the FD12P and Sentry  $Vis$ ) are given based on the WMO MOR definitions.

### b) Nighttime definition of $Vis$

The nighttime  $Vis$  ( $Vis_n$ ) is obtained (Rasmussen et al., 1999) using the simplified Allard's law as

$$Vis_n = \frac{I_o}{C_{DB}} \exp(-\beta_{ext}Vis_n), \quad (5)$$

where  $C_{DB}=0.084$  miles<sup>-1</sup> and  $I_o=25$  candela. Comparing  $Vis_d$  [km] versus  $Vis_n$  [km], using the assumed coefficients in Eq. 5, a simplified equation can be obtained as

$$Vis_n = 1.8507Vis_d^{0.814}. \quad (6)$$

For forecasting applications, measurements done with instruments (if they do not perform processing internally) should be converted to nighttime visibilities using Eq. 6.

## 3. MEASUREMENTS

Surface observations during the FRAM field project were collected at the Center for Atmospheric Research Experiment (CARE) site near Toronto, Ontario during the winter of 2005-2006 and in Lunenburg, Nova Scotia during the summers of 2006 and 2007 (Gultepe et al., 2008). The main observations used in the analysis were fog droplet spectra from a fog measuring device (FMD; DMT Inc.),  $Vis$  and precipitation rate ( $PR$ ) from the VAISALA FD12P all-weather sensor and the OTT laser based optical disdrometer called ParSiVel

(Particle Size and Velocity), and  $RH_w$  together with temperature ( $T$ ) from the Campbell Scientific HMP45 sensor. Liquid water path ( $LWP$ ) and liquid water content ( $LWC$ ) were obtained from a microwave radiometer (MWR). Fog coverage and some microphysical parameters such as droplet size, phase, and  $LWP$  were also obtained from satellites (e.g. GOES and MODIS products). Details on some of the instruments can be found in Gultepe and Milbrandt (2007) and are discussed here briefly.

The FD12P Weather Sensor is a multi-variable sensor for automatic weather stations and airport weather observing systems (VAISALA Inc.). The sensor combines the functions of a forward scatter  $Vis$  meter and a present weather sensor. Fig. 2 shows an example of FD12P measurements for the June 18 2006 case. This sensor also measures the accumulated amount and instantaneous  $PR$  for both liquid and solid precipitations, and provides the  $Vis$  and precipitation type related weather codes given in the World Meteorological Organization (WMO) standard SYNOP and METAR messages.

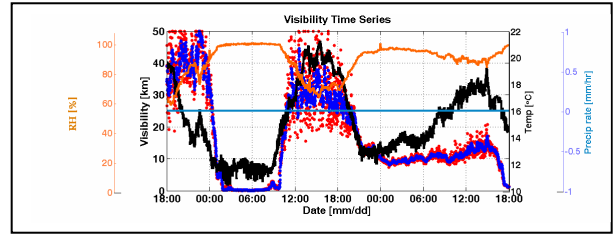


Fig. 2: Time series of FD12P measurements for a fog event occurred during June 18 2006.

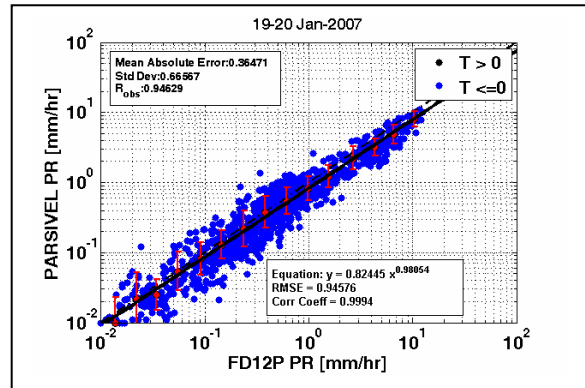


Fig. 3: The OTT Parsivel distrometer  $PR$  versus FD12P  $PR$  for a snow event during the winter of 2007.

The FD12P detects precipitation droplets from rapid changes in the scatter signal. The droplet data are then used to estimate precipitation rate and amount. Based on the manufacturer's specifications, the

accuracy of the FD12P measurements for  $Vis$  and  $PR$  are approximately 10% and  $0.05 \text{ mm h}^{-1}$  respectively. The  $PR$  measurements from both the FD12P and OTT distrometer for a snow event are shown in Fig. 3. This suggests that FD12P  $PR$  measurements are within acceptable limits and they have been used in the analysis.

The OTT ParSiVel is also designed to operate under all-weather conditions (Löffler-Mang and Joss, 2000; Löffler-Mang and Blahak, 2001). This instrument can provide information on present weather, optical rain gauging, particle spectrum, visibility, and radar reflectivity. It has a built-in heating device to reduce the effects of freezing and frozen precipitation accreting on the critical surfaces on the instrument. The particles are classified into 32 classes of sizes and velocities. The basic measuring range for velocity and size is from 0 to  $20 \text{ m s}^{-1}$ , and 0.2 mm to 25 mm, respectively. According to the manufacturer, the rain rate error is approximately 5%. The accuracy of the snow precipitation rate is discussed later.

The fog-related microphysics parameters e.g.  $LWC$ , size, and droplet number concentration ( $N_d$ ) were calculated from the FMD spectra, and an example of the fog droplet spectra for the fog event on June 18 2006 is given in Fig. 4.

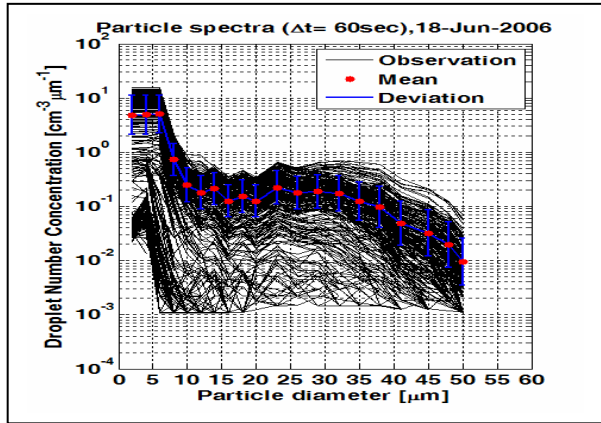


Fig. 4: Fog droplet spectra from the FMD instrument on June 18 2006.

#### 4. GEM-REG PHYSICS AND SIMULATION

The 18 June 2006 case was simulated using the Canadian operational Global Environmental Multiscale (GEM) numerical weather prediction model. The model dynamics are discussed in detail by Côté et al. (1998). GEM has a comprehensive physics package which includes a planetary boundary layer scheme based on turbulent kinetic energy, implicit (explicit) vertical (horizontal)

diffusion, and a detailed land-surface scheme. The solar and infrared radiation package is fully interactive with the model clouds. Subgrid-scale convection is treated by the Kain and Fritsch (1993) convective parameterization. The Sundqvist et al. (1989) condensation scheme is used to treat grid-scale clouds. This cloud scheme includes a prognostic equation for a single variable representing non-sedimenting condensed water mass (liquid or frozen). The model uses 58 unevenly spaced terrain-following vertical levels.

#### 5. METHOD AND PREVIOUS STUDIES

In this section,  $Vis$  parameterizations developed for various hydrometeors and  $RH$  are given and compared to others that were previously reported.

##### a) $Vis$ - $RH$ relationships

The  $Vis$ - $RH$  relationships based on percentiles were obtained using observations from the FD12P  $Vis$  and Campbell  $RH_w$  measurements. A single fit (applied to means) cannot always be valid for different environments; therefore, the fits for percentiles should be used to more accurately estimate  $Vis$ . The  $Vis$  versus  $RH_w$  fits from other studies are summarized in Table 1. In general, the  $Vis$ - $RH_w$  relationship obtained in the present work was significantly different from the one used in the RUC model (Smirnova et al., 2000; Gultepe et al., 2008).

Table 1:  $Vis$  versus  $RH_w$  relationships based on the various field programs and RUC model.

Relationship	Reference
$Vis_{RUC} = 60 \exp(-2.5 * (RH_w - 15) / 80)$	RUC model
$Vis_{FRAM-C} = -41.5 \ln(RH_w) + 192.3$	Gultepe et al. (2006a)
$Vis_{AIRS} = -0.018 RH_w^2 + 1.46 RH_w + 30.8$	Gultepe et al. (2006a)
$Vis_{FRAM-L(95\%)} = -0.00012 RH_w^{2.70} + 27.45$	FRAM
$Vis_{FRAM-L(50\%)} = -5.19 * 10^{-10} RH_w^{5.44} + 40.10$	FRAM
$Vis_{FRAM-L(5\%)} = -9.68 * 10^{-14} RH_w^{7.19} + 52.20$	FRAM

##### b) $Vis$ for fog

###### i) Liquid fog

Gultepe et al (2006b) developed a parameterization for  $T > 0^\circ\text{C}$  and  $RH_w \sim 100\%$  that is based on both  $LWC$  and  $N_d$ . The current RUC model uses a  $Vis$ - $LWC$  relationship for fog visibility (Stoelinga and Warner, 1999). Using information that  $Vis$  decreases with increasing  $N_d$  and  $LWC$ , a relationship between  $Vis_{obs}$  and  $(LWC \cdot N_d)^{-1}$  called the “fog index” is determined as

$$Vis_{obs} = \frac{1.002}{(LWC \cdot N_d)^{0.6473}} \quad (7)$$

This fit suggests that  $Vis$  is inversely related to both  $LWC$  and  $N_d$ . The maximum limiting  $LWC$  and  $N_d$

values used in the derivation of Eq. 7 are about  $400 \text{ cm}^{-3}$  and  $0.5 \text{ g m}^{-3}$ , respectively. The minimum limiting  $N_d$  and  $LWC$  values are  $1 \text{ cm}^{-3}$  and  $0.005 \text{ g m}^{-3}$ , respectively. In Eq. 7,  $N_d$  can be fixed as  $100 \text{ cm}^{-3}$  for marine environments and  $200 \text{ cm}^{-3}$  for continental fog conditions. These values of  $N_d$  are traditionally used in modeling applications which cannot be valid for all environmental conditions.

### ii) Ice fog and Vis parameterization

Ice fog forecasting is usually not performed with forecasting models because ice water content ( $IWC$ ) and ice crystal number concentration ( $N_i$ ) are not accurately obtained from existing microphysics algorithms (Gultepe et al., 2001). If both parameters were available from a high-resolution fog/cloud model, they could be used for ice fog forecasting. Ice fog occurs commonly in northern latitudes when  $T$  is below  $-15^\circ\text{C}$  (based on the first author's observations in Barrow, Alaska). The formation of ice fog usually occurs when the  $RH$  becomes saturated with respect to ice ( $RH_i$ ) with no precipitation. Ice fog occurs because of deposition nucleation process that depends on nuclei size and concentration, and temperature. Previous reports suggested that liquid droplets can be found at  $T$  down to about  $-40^\circ\text{C}$  but it is not common to find droplets colder than  $-20^\circ\text{C}$ . Using aircraft observations collected during the First International Regional Experiment-Arctic Cloud Experiment (FIRE-ACE) Gultepe et al., 2003 found that frost point temperature ( $T_f$ ) can be related to dew point temperature ( $T_d$ ) as:

$$T_f = T_d + \Delta f, \quad (8)$$

where  $T_d$  [ $^\circ\text{C}$ ] and  $T_f$  [ $^\circ\text{C}$ ] were obtained using LiCOR instrument humidity measurements (Gultepe et al., 2003) and their difference is parameterized as:

$$\Delta f = p_1 T_d^3 + p_2 T_d^2 + p_3 T_d + p_4, \quad (9)$$

where  $p_1=0.000006$ ;  $p_2=-0.0003$ ;  $p_3=-0.1122$ ; and  $p_4=0.1802$ . If  $T_d$  is known, then  $T_f$  [ $^\circ\text{C}$ ] is calculated using Eqs. 8 and 9. The following equation is given for saturated vapor pressure by Murray (1967) as

$$e_s = 6.1078 \exp\left[\frac{a(T - 273.16)}{(T - b)}\right], \quad (10)$$

where  $T$  [K],  $e$  [mb],  $a=21.8745584$  (17.2693882);  $b=7.66$  (35.86) over the ice (water) surface. Then, using  $T_f$  and  $T$ , relative humidity with respect to ice ( $RH_i$ ) is obtained from the following equation

$$RH_i = \frac{e_i(T_d + \Delta f)}{e_{si}(T)}. \quad (11)$$

If  $RH_w$  and  $T$  are known, then  $T_d$  is calculated using an equation similar to Eq. 11 but for water. Using Eqs. 8-11,  $RH_i$  is then calculated. If  $RH_i$  is greater

than approximately 95%,  $T < -10^\circ\text{C}$ , and no precipitation occurs, then ice fog regions can be obtained from model simulations. If  $IWC$  is prognostically obtained, then  $Vis$  for ice fog, assuming that  $N_i$  and mean equivalent mass diameter ( $d$ ) are known, can be obtained (Ohtake and Huffman, 1969) as:

$$Vis = \frac{1}{3} \left[ 3.2 \frac{IWC}{N_i} \right]^{1/3} - 1.5\bar{d} \quad (12)$$

Eq. 12 shows how  $Vis$  changes with  $IWC$ ,  $N_i$ , and  $d$ . In this work, it is suggested that  $N_i$  and  $d$  can be taken as  $200 \text{ cm}^{-3}$  and  $7.2 \mu\text{m}$  (for high  $IWC$  e.g.  $>0.1 \text{ g m}^{-3}$ ), and as  $80 \text{ cm}^{-3}$  and  $4.5 \mu\text{m}$  (for low  $IWC$  e.g.  $>0.01 \text{ g m}^{-3}$ ). If ice crystals form due to deposition of vapor directly onto ice nuclei at cold  $T$ ,  $N_i$  can be parameterized as a function of  $RH_i$ . A relationship between  $N_i$  and  $RH_i$  for ice fog does not currently exist. Note that Eq. 12 and its validity will be verified using measurements from the FRAM-ISDAC project which took place over Barrow, Alaska, US, during April of 2008.

### c) Vis for rain and snow from previous works

Previously reported  $Vis$  parameterizations for rain and snow have been used in modeling studies. In Table 2, the subscript  $MP$  presents the Marshall-Palmer distribution (Marshall and Palmer, 1948). The  $SS$  signifies the Sekhon and Srivastava (1970 and 1971) works for snow and rain, respectively. The  $ST$  represents the Stalla brass (1985) study. The  $LWC$  and  $IWC$  are in the units of [ $\text{g m}^{-3}$ ] and  $\beta$  in [ $\text{km}^{-1}$ ]. The  $\beta_s$  represents the extinction coefficient given by Seagraves (1984) work that is based on Muench and Brown (1977). Details on this can be found in Gultepe et al (2008). The relationships given in Table 2 are not unique because the  $PR$  variability with  $Vis$  is large (Gultepe et al. 2008; Rasmussen et al., 1999).

Table 2: Visibility versus precipitation rates for rain and snow from various studies.

Parameterizations	Notes
RUC model for rain	
$Vis_{MP} = -\log(0.02) / \beta$	$LWC_{MP} = 0.072PR^{0.88}$
$\beta = 2.24LWC^{0.75}$	$LWC_{SS} = 0.052PR^{0.94}$
RUC model for snow	
$Vis_{SS} = -\log(0.02) / \beta_{ST}$	$IWC_{SS} = 0.25PR^{0.86}$
$\beta_{ST} = 10.36IWC^{0.7776}$	
Seagraves (1984) for snow	
$Vis_s = -\log(0.02) / \beta_s$	$\beta_s = 2.52PR^{0.77}$

**d) Vis for snow and rain using probability curves**

The *Vis* for rain and snow cannot be solely obtained from *Vis-PR* mean relationships because of variability in particle spectra. For this reason, percentiles (5%, 95%, 50% values) for *Vis* in rain and snow conditions can be obtained as given in Table 3. If the drizzle phase can be specified from the model, then Eq. 5 in Table 3 can be used for calculating *Vis*. This was summarized in Gultepe et al. (2008).

Table 3: Visibility versus precipitation rates for rain ( $Vis_R$ ), drizzle ( $Vis_{DR}$ ), and snow ( $Vis_S$ ) from the FRAM observations.

Precip type	$PR=[\text{mm h}^{-1}]; Vis=[\text{km}]$
Rain (mean)	$Vis_R = -4.116PR^{0.176} + 9.01$
Rain (50%)	$Vis_R = -2.648PR^{0.256} + 7.65$
Rain (95%)	$Vis_R = -0.447PR^{0.394} + 2.28$
Rain (5%)	$Vis_R = -863258PR^{0.003} + 87419$
Drizzle (mean)	$Vis_{DR} = -2.658PR^{-0.526} + 6.541$
	$PR=[\text{mm h}^{-1}]; Vis=[\text{km}]$
Snow (mean)	$Vis_S = 1.10PR^{-0.701}$
Snow (50%)	$Vis_S = 1.063PR^{-0.682}$
Snow (95%)	$Vis_S = 0.617PR^{-0.591}$
Snow (5%)	$Vis_S = 1.654PR^{-0.795}$

**e) New method against Vis-PR relationships**

Measurements from the OTT disdrometer were collected during the winter of 2007-2008 and used in the analysis. From the OTT disdrometer measurements, both rain and snow related parameters e.g.  $LWC$ ,  $IWC$ ,  $N_d$ ,  $N_i$ , particle size, terminal velocities, extinction coefficients,  $PR_R$ , and  $PR_S$  were obtained for particle sizes >400 microns. Similar to fog *Vis*,  $Vis_R$  and  $Vis_S$  parameterizations were obtained for a snow/rain event (Fig. 5) which occurred on December 3 2007, respectively, as

$$Vis_R = 1.381 \left( \frac{1}{LWC \cdot N_{Rt}} \right)^{0.5633}, \quad (13)$$

and

$$Vis_S = 29.011 \left( \frac{1}{IWC \cdot N_{St}} \right)^{0.4433}. \quad (14)$$

While  $N_{Rt}$  (total number concentration of rain drops) and  $N_{St}$  (total number concentration of snow flakes) are related to various meteorological and thermodynamical parameters, here they are assumed only to be related to  $PR$ . This is better than

using a fixed value as is done in the current forecasting models. Using the OTT disdrometer measurements,  $N_{Rt}$  and  $N_{St}$  versus  $PR$  parameterizations (Fig. 6) are obtained, respectively, as

$$N_{Rt} = 3.2PR_R^{0.22} \quad (15)$$

and

$$N_{St} = 8.42PR_S^{0.35}. \quad (16)$$

Note that these relationships can change depending on precipitation process and snow particle shape.

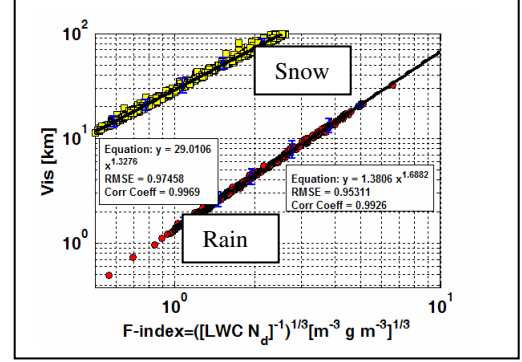


Fig. 5: *Vis* versus fog index for a precipitation event on December 3 2007.

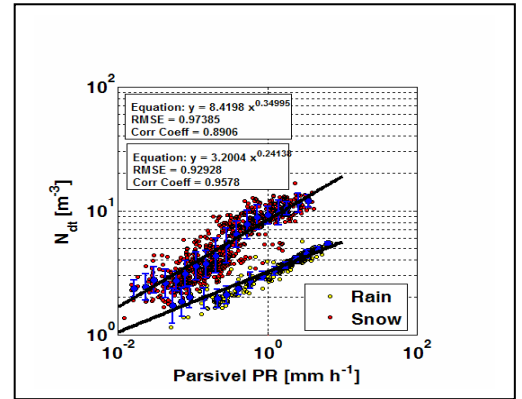


Fig. 6: Rain drop (snow crystal) number concentration versus  $PR$  for rain (snow) during a precipitation event on December 3 2007.

**f) Integration of extinctions coefficients**

Equations given for  $Vis-f(LWC, N_d)$  (for rain and warm fog),  $Vis-f(IWC, N_i)$  (for snow and cold fog), and  $Vis-RH_w$  parameterizations can be used to obtain integrated *Vis* values. In the case of both fog and precipitation occurring together, calculated *Vis* values are first converted to extinction coefficients ( $\beta_{ext}$ ) using Eq. 1, then, an integrated extinction coefficient is obtained as

$$\beta_{int} = \beta_{RH_w} + \beta_{LWC;IWC} + \beta_{R;S}. \quad (17)$$

The final value of  $Vis$  is then calculated using Eq. 1 which utilizes  $\beta_{int}$ .

## 6. RESULTS

In this section, results from the June 18 2006 marine fog case are presented. At the end of the fog episode, around noon local time, some drizzle occurred but it was not considered in the analysis.

### a) Synoptic Conditions

The fog event on June 18 lasted approximately 7 h. Several GOES images showed fog areas over the project site (Fig. 7). Fig. 7 shows the foggy areas in green obtained using a technique given by Gulpepe et al (2007). Fog coverage was more over land during the early hours of the event. At about 10 AM, the fog moved over the ocean, and then it moved over land again after midnight the following day. A skewT-LogP diagram (Fig. 8) from the NOAA MAPS analysis valid at 9 AM showed that lowest boundary layer was relatively saturated and winds were from southwest, resulting in conditions conducive for fog formation.

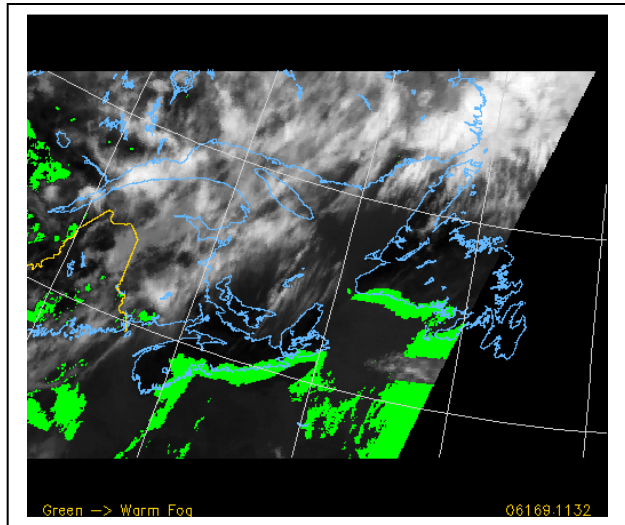


Fig. 7: the GOES fog product (green color) over FRAM project site at 06:32 EST on June 18 2006.

### b) Microphysical observations

The fog event on June 18 started to occur at 02:00 AM in the morning (Fig. 2). It lasted about 7 hours and  $Vis$  was less than 200-300 m. The FMD  $N_d$  and  $Vis$  time series are shown in Fig. 9a and 9b, respectively. The  $Vis$  versus  $N_d$  and  $LWC$ , representing 1-minute averaging with standard deviation, are shown in Figs. 9c and 9d, respectively.  $Vis$  nonlinearly decreases with both

increasing  $N_d$  and  $LWC$ , suggesting that  $Vis$  is a function of both parameters. Fog droplet settling rate and  $Vis$  versus fog index [ $1/(LWCN_d)$ ] are shown in Figs. 9e and 9f, respectively. These plots suggest that droplet settling rate is a function of both  $LWC$  and  $N_d$ . The last two plots show the  $Vis$  versus reflectivity factor ( $Z$ ) (Fig. 9g) and  $Z$  versus  $LWCR_{eff}^2$  (Fig. 9h). Knowing  $Z$  for fog droplets and assuming a characteristic particle size (e.g. effective size for fog droplets), fog  $LWC$  can be obtained from a mm radar.

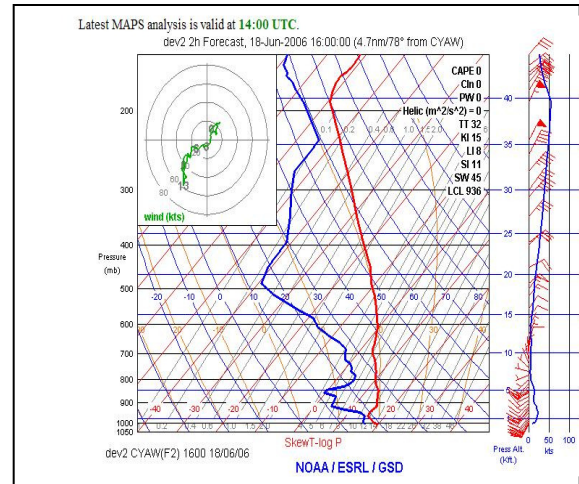


Fig. 8 SkewT-LogP diagram from the MAPS analysis valid at 09:00 AM EST.

### c) GEM-REG simulations

Figure 10a depicts the simulated field of liquid water content ( $LWC$ ) at the second lowest model level (approximately 140 m above the surface) at 10:00 UTC on 18 June 2006. Near Lunenburg Bay (the south-west region in Fig. 10a), the simulated  $LWC$  values are between 0.10–0.20  $g\ m^{-3}$ . The visibility corresponding to this simulated liquid fog is calculated using Eq. 7. Since the droplet number concentration is not a prognostic variable in the Sundqvist cloud scheme,  $N_d=80\ cm^{-3}$  is assumed in the simulations, which is typical for a maritime air mass. In fact, this value can change with T (Gulpepe and Isaac, 2004). The  $Vis$  from the simulation is shown in Fig. 10b and it was about 0.20–0.40 km at the Lunenburg Bay area. Fig. 10c shows the  $RH_w$  over the projected area. Along the shoreline,  $RH_w$  is found to be greater than 95% which corresponds to a saturated layer with respect to water over the 15 km scale. Gulpepe et al. (2008) stated that  $Vis$  can be about 1-2 km if no  $LWC$  exists which corresponds well with the satellite based fog regions shown in Fig. 7.

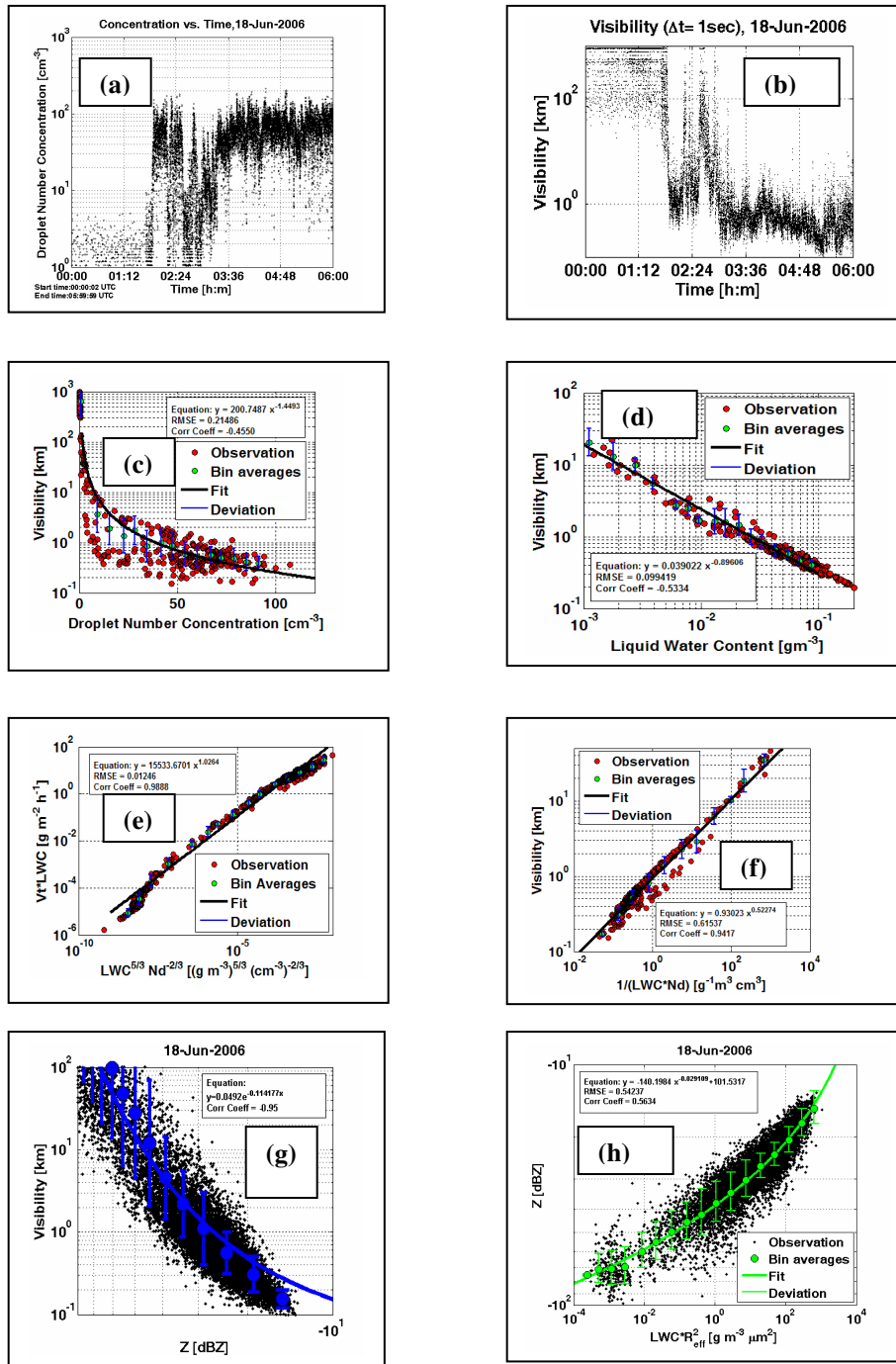


Fig. 9: Microphysical data representing a marine fog case from the FMD instrument collected during June 18 2006.

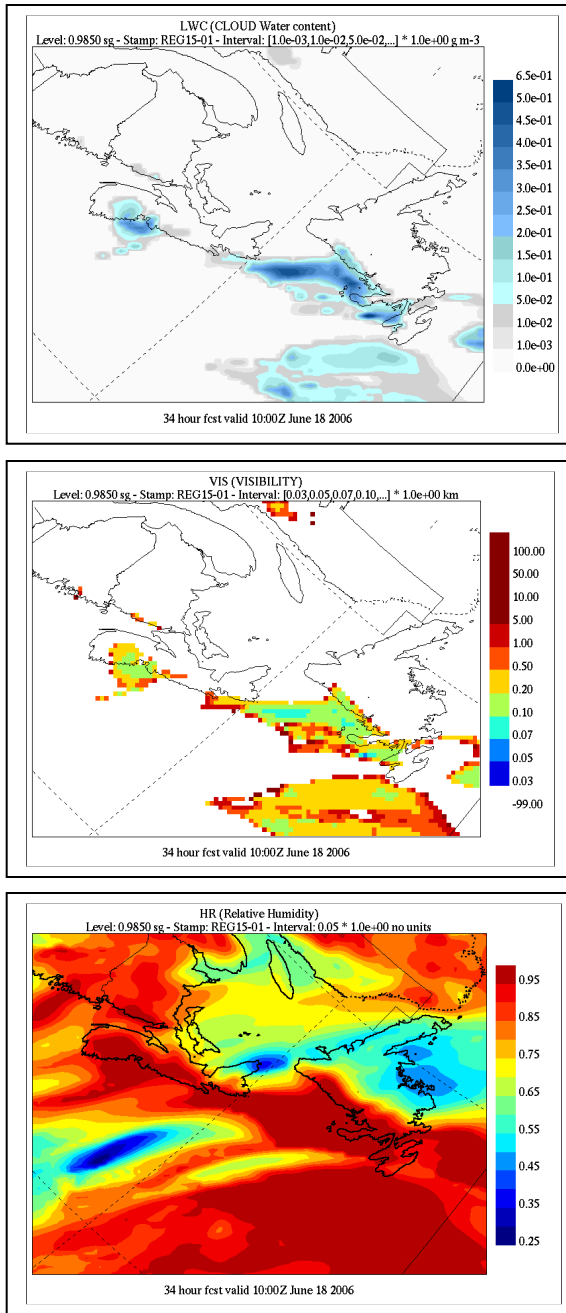


Fig. 10: GEM model simulation of (a)  $LWC$  [ $g\ m^{-3}$ ] and (b)  $Vis$  [km], and  $RH_w$  (c) at the second lowest model level, valid at 10:00 UTC on 18 June 2006.

## 7. DISCUSSIONS

To accurately forecast/nowcast fog VIS, accurate model output parameters are required e.g.  $LWC$ ,  $N_d$ ,  $RH$ , and  $PR$ . If model output values for rain, snow,  $RH$ , and  $LWC$  are not accurate better than 20-30%, the uncertainty in  $Vis$  can be as high as 50% (Gultepe et al, 2006b). If fog  $LWC$  and  $N_d$  are not accurately known from a model at the levels closest

to the surface, then  $Vis$  based on other parameters e.g.  $PR$  or  $RH$ , or both, cannot be used to obtain accurate  $Vis$ . Fog  $LWC$  and  $N_d$  are the major factors required for accurate  $Vis$  calculations and they should be obtained to an accuracy of about 10-20%.

The  $Vis$  probability curves need to be tested for various geographical regions. The grid-point values of  $Vis$  obtained from the NWP models do not necessarily correspond directly to point measurements due to issues of model grid-spacing and spatial averaging. Model-based results should also consider subgrid-scale variability of  $Vis$ ,  $PR$ ,  $RH_w$ , and condensed water content. In this work, parameterizations (obtained from *in-situ* measurements) used in the RUC model were applied for comparisons without simulations (Fig. 11). This figure suggests that  $Vis$  should also be dependent on some other parameters rather than only  $PR$ , as suggested by Eqs. 13 and 14.

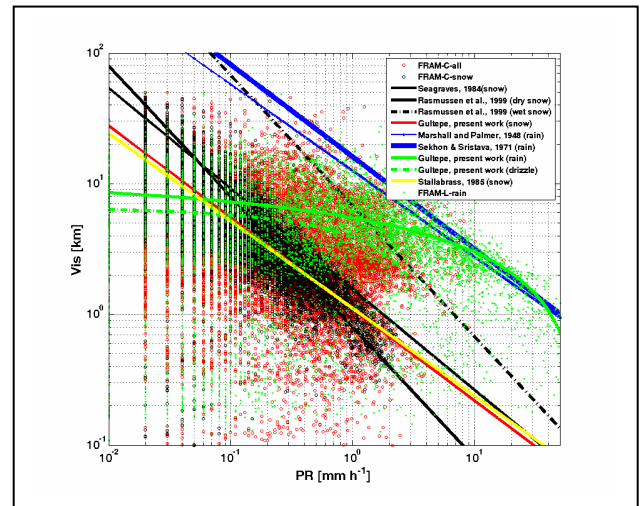


Fig. 11: The  $Vis$  versus  $PR$  for rain (green dots and red dots), snow (black dots), drizzle, and for previous studies (Table 3). The results from the present work (Table 2) are also shown. The  $Vis$  and  $PR$  are obtained from FD12P measurements.

Marine fog nowcasting/forecasting needs detailed surface fog measurements, high-resolution forecasting model outputs, and satellite observations. Integration of the data from various platforms can be used to obtain accurate fog  $Vis$ . Fig. 12 shows intensity of  $Vis$  (from July 11 to October 31 2007) related to 24 h back trajectories which ended up at Halifax International Airport, Nova Scotia. It is seen that most of the air parcels coming from the south and southwest sectors result in low  $Vis$  values. This suggests that analysis of sea

surface temperature and back trajectories can help to better nowcast/forecast marine fog conditions.

The simulation results suggest that visibility can be estimated by using parameters produced from the cloud schemes. Applying observation-based parameterizations such as Eq. 7 as an alternative to those based on specific hydrometeor size distribution functions, can be used to compute extinction coefficients directly (as in Eq. 2). Researchers in Environment Canada are currently working on the implementation of a more detailed two-moment version of the cloud microphysics scheme (Milbrandt and Yau, 2005a,b) to treat grid-scale clouds in the high-resolution version (2.5-km grid-spacing) of the GEM model. In this scheme, both  $LWC$  and  $N_d$  are independent prognostic variables. This should allow a more flexible application of the visibility parameterization of Eq. 7, without the restriction of prescribing a value of  $N_d$ .

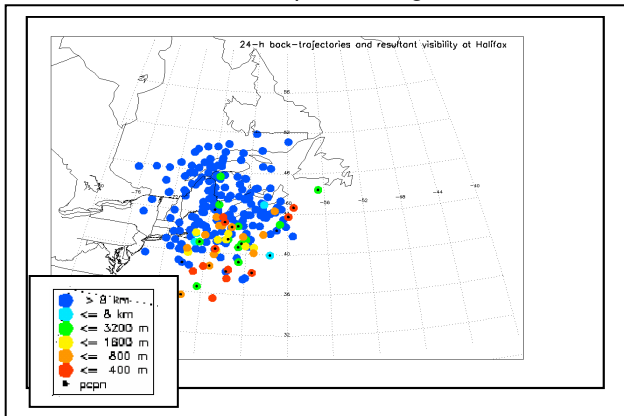


Fig. 12: Visibility intensity at the Halifax International Airport corresponding to source locations of 24-h back trajectories from July 11 to October 31 2007.

## 8. CONCLUSIONS

Fog  $Vis$  due to rain/snow is strongly related to their mass content ( $MC$ ) and number concentrations ( $N$ ) rather than  $PR$ . These two parameters play an important role in parameterizations of  $Vis$ . Using a case study,  $Vis$  as a function of  $MC$  and particle number concentration was suggested for both rain (Eq. 13) and snow (Eq. 14) conditions. These equations may represent rain and snow events with different microphysics, however this needs to be validated.

For snow conditions, particle shape and phase (e.g. wet snow) affect  $Vis$  as much as number concentration. From the definition of extinction, particle surface area is related to snowflake habit, which affects  $Vis$  significantly. Particle shape effect in  $Vis$  calculations can be considered using terminal

velocities, particle size, or both. The combination of  $LWC$  and snowflake size (or  $N_i$ ) can be used for  $Vis$  calculations (e.g. Eqs.12 and 14).

The results from the GEM-REG simulation suggest that the microphysics parameterization presented, which includes  $N_d$ , can improve  $Vis$  values from forecasting models. A new microphysical scheme to be used in the GEM limited area model (LAM) (Milbrandt and Yau, 2005a,b) will provide both  $N_d$  and  $LWC$  values in a prognostic way that should lead to more accurate calculations of  $Vis$  values.

Finally, back trajectories of air masses together with other data sets e.g. satellite based algorithms, model based products, and ocean surface T data can be integrated to better forecast/nowcast marine fog and its visibility.

An ice fog visibility parameterization as suggested by Ohtake and Huffman (1969) was modified for model simulations and an ice fog area coverage detection based on a new parameterization of  $RH_i$  has been suggested. These can be used in nowcasting/forecasting applications. A new equation is given for the frost point  $T$  calculation that can be used in  $RH_i$  calculation over a model grid area. The ice fog  $Vis$  parameterization (Ohtake and Huffman, 1969) needs to be verified and this will be done using the new observations obtained during FRAM-ISDAC field project which took place over Barrow, Alaska, US, during April of 2008.

## Acknowledgements

Funding for this work was provided by the Canadian National Search and Rescue Secretariat and Environment Canada. Authors are thankful to M. Wasey and R. Reed of Environment Canada for technical support.

## References

- Benjamin, S.G., D. Devenyi, S.S. Weygandt, K.J. Brundage, J.M. Brown, G.A. Grell, D. Kim, B.E. Schwartz, T.G. Smirnova, T.L. Smith, and G.S. Manikin, 2004: An hourly assimilation/forecast cycle: The RUC. *Mon. Wea. Rev.*, **132**, 495-518.
- Bott, A., U. Sievers, and W. Zdunkowski, 1990: A radiation fog model with a detailed treatment of the interaction between radiative transfer and fog microphysics, *J. Atmos. Sci.*, **47**, 2153–2166.
- Côté, J., S. Gravel, A. Methot, A. Patoine, M. Roach, and A. Staniforth, 1998: The operational CMC-MRB

- Global Environmental Multiscale (GEM) model: Part I - Design considerations and formulation. *Mon. Wea. Rev.*, **126**, 1373-1395.
- Gadher, D, and Baird, T, cited 2007: Airport dash as the fog lifts, *The Sunday Times*, posted online 24 December 2006. [Available online at <http://www.timesonline.co.uk/article/0,,2087-2517675.html>.]
- Gultepe, I., G. A. Isaac, and S. G. Cober, 2001: Ice crystal number concentration versus temperature for climate studies. *Inter. J. of Climatology*, **21**, 1281-1302.
- Gultepe, I., G. Isaac, A. Williams, D. Marcotte, and K. Strawbridge, 2003: Turbulent heat fluxes over leads and polynyas and their effect on Arctic clouds during FIRE-ACE: Aircraft observations for April 1998. *Atmosphere and Ocean*, **41(1)**, 15-34.
- Gultepe, I., and G. Isaac, 2004: An analysis of cloud droplet number concentration ( $N_d$ ) for climate studies: Emphasis on constant  $N_d$ , *Quart. J. Roy. Meteor. Soc.*, **130**, Part A, 2377-2390.
- Gultepe, I., and G. A. Isaac, 2006 Visibility versus precipitation rate and relative humidity. AMS 12<sup>th</sup> Cloud Physics Conference, July 9-14, 2006, Madison, Wisconsin, USA, Prints in CD print, p255.
- Gultepe, S.G. Cober, P. King., G. Isaac, P. Taylor, and B. Hansen, 2006a: The Fog Remote Sensing and Modeling (FRAM) field project and preliminary results, AMS 12<sup>th</sup> Cloud Physics Conference, July 9-14, 2006, Madison, Wisconsin, USA, Print in CD, P4.3.
- Gultepe, I., M. D. Müller, and Z. Boybeyi: 2006b: A new visibility parameterization for warm fog applications in numerical weather prediction models, *J. Appl. Meteor.* **45**, 1469-1480
- Gultepe, I., and J. A. Milbrandt, 2007: Microphysical observations and mesoscale model simulation of a warm fog case during FRAM project, *J. of Pure and Applied Geophy.*, **164**, 1161-1178.
- Gultepe, I., Pagowski, M., and Reid, J., 2007: Using surface data to validate a satellite based fog detection scheme, *Weather and Forecasting*, **22**, 444-456.
- Gultepe, I., S.G. Cober, G. Pearson J. A. Milbrandt B. Hansen, G. A. Isaac, S. Platnick, P. Taylor, M. Gordon, J. P. Oakley, 2008: The fog remote sensing and modeling (FRAM) field project and preliminary results. *Bull. Amer. Meteor. Soc.*, Conditionally accepted.
- Jacobs, W., Vesa Nietosvaara, Andreas Bott, Jörg Bendix, Jan Cermak, Silas Chr. Michaelides, and Ismail Gultepe, 2007: COST Action 722, Earth System Science and Environmental Management, *Final report on Short Range Forecasting Methods of Fog, Visibility and Low Clouds*. Available from COST-722, European Science Foundation, 500 pp.
- Kain, J. S. and J. M. Fritsch, 1993: Convective parameterization for mesoscale models: The Kain-Fritsch scheme. The Representation of Cumulus Convection in Numerical Models, Meteor. Monogr., No. **46**, *Amer. Meteor. Soc.*, 165-177.
- Löffler-Mang, M., and J. Joss, 2000: An optical disdrometer for measuring size and velocity of hydrometeors. *J. Atmos. Ocean. Tech.*, **17**, 130-139.
- Löffler-Mang, M., and U. Blahak, 2001: Estimation of the equivalent radar reflectivity factor from measured snow size spectra. *J. Appl. Meteor.*, **40**, 843-849.
- Marshall, J. S., and W. M. K. Palmer, 1948: The distribution of raindrops with size. *J. Meteor.*, **17**, 1054-1061.
- Milbrandt, J. A. and M. K. Yau, 2005a: A multi-moment bulk microphysics parameterization. Part I: Analysis of the role of the spectral shape parameter. *J. Atmos. Sci.*, **62**, 3051-3064.
- Milbrandt, J. A. and M. K. Yau, 2005b: A multimoment bulk microphysics parameterization. Part II: A proposed three-moment closure and scheme description. *J. Atmos. Sci.*, **62**, 3065-3081.
- Muench, H. S., and H. A. Brown, 1977: Measurements of visibility and radar reflectivity during snowstorms in the AFGL mesonet. Environmental Res. Paper AFGL-TR-77-0148, 36 pp. [Available from the Meteorology Division, Project 8628, Air Force Geophysics Laboratory, Hanscom AFB, MA 01731.].
- Murray, F. W., 1967: On the computation of saturation vapor pressure. *J. App. Meteor.*, **6**, 203-204.
- Ohtake, T. and P.J. Huffman, 1969: Visual Range in Ice Fog, *J. of App. Meteor.*, **8**, 499-501.

- Rasmussen, R. M., J. Vivekanandan, J. Cole, B. Myers, and C. Masters, 1999: The estimation of snowfall rate using visibility. *J. Applied. Meteor.*, **38**, 1542-1563.
- Seagraves, M.A., 1984: Precipitation Rate and Extinction in Falling Snow, *J. Atmos. Sci.*, **41**, 1827-1835
- Sekhon, R. S., and R.C. Srivastava, 1970: Snow size spectra and radar reflectivity. *J. Atmos. Sci.*, **27**, 299–307.
- Sekhon, R. S., and R.C. Srivastava, 1971: Doppler radar observations of drop-size distributions in a thunderstorm. *J. Atmos. Sci.*, **28**, 983–994.
- Stallabrass, J. R., 1985: Measurements of the concentration of falling snow. Tech. Memo., 140, *Snow Property Measurements Workshop*. Lake Louise, AB, Canada, National Research Council Canada. 20 pp.
- Smirnova, T.G., S.G. Benjamin, and J.M. Brown, 2000: Case study verification of RUC/MAPS fog and visibility forecasts. Preprints, 9th Conf. on Aviation, Range, and Aerospace Meteorology, AMS, Orlando, 31-36.
- Stoelinga, M. T., and T. T. Warner, 1999: Nonhydrostatic, meso-beta scale model simulations of cloud ceiling and visibility for an east coast winter precipitation event. *J. Appl. Meteor.*, **38**, 385-404.
- Sundqvist, H., E. Berge, and J. E. Kristjánsson, 1989: Condensation and cloud parameterization studies with a mesoscale numerical weather prediction model. *Mon. Wea. Rev.* **117**, 1641-1657.
- Westcott, N. E., 2007: Some aspects of dense fog in the Midwestern United States. *Weather and Forecasting*, **22**, 457-465.